Available online at www.sciencedirect.com

ScienceDirect

Procedia CIRP 82 (2019) 344–349

www.elsevier.com/locate/procedia

17th CIRP Conference on Modelling of Machining Operations

Material behaviour at low temperatures for calibrating cryogenic machining numerical simulations

R. Bertolini[a], S. Bruschi[a*], A. Ghiotti[a], G. Haugou[b], H. Morvan[b], L. Dubar[b]

[a]*Department of Industrial Engineering, University of Padova, Via Venezia 1, 35131, Padova, Italy*
[b] *LAMIH, University of Valenciennes and Hainaut-Cambrésis, Malvache building, Le Mont Houy, F59313 Valenciennes, France*

* Corresponding author. Tel. +39 049 8276821. *E-mail address:* stefania.bruschi@unipd.it

Abstract

Recently, cryogenic machining of difficult-to-cut alloys has been adopted to increase tool life and improve the machined components surface integrity. Numerical models of cryogenic machining are being developed to evaluate the influence of the different process parameters. Up to now, their calibration in terms of material flow stress is fulfilled using data at conventional temperatures, whereas the material sensitivity to temperatures lower than the environment one should be taken into account. To this regard, the paper objective is to present material data, obtained through a newly developed Split Hopkinson Tension Bar, at cryogenic temperatures and high strain rates to properly calibrate cryogenic machining numerical models.

Peer-review under responsibility of the scientific committee of The 17th CIRP Conference on Modelling of Machining Operations

Keywords: Cryogenic machining; Titanium; Temperature; Stress

1. Introduction

In recent years, cryogenic machining has been extensively applied to the so-called difficult-to-cut metal alloys with the twofold objective of reducing the tool wear and increasing the part in-service performances [1]. The former is fulfilled thanks to the drastic reduction of the cutting temperature, which, in turn, limits adhesion and diffusion wear phenomena to a great extent [2]; whereas, the latter is usually achieved thanks to the attainment of machining-altered layer characterized by ultra-fined microstructure and compressive residual state of stress [3]. The influence of the cutting parameters and of the layout of the liquid nitrogen delivery system can be evaluated by means of either machining trails or numerical simulations. While the former are costly and time-consuming, the latter are still far from being an established procedure due to the difficulties that can be encountered in calibrating the numerical models devoted to machining operations. Attempts for the numerical modelling of cryogenic machining have been done recently, as in [4][5] where flow stress data of the workpiece material were coupled with microstructural features evolution to give a proper description of the machined surface integrity. Usually, flow stress data for machining simulations are gained from tests carried out at elevated strain rate values, being the latter relevant to cutting operations, making use of either tensile or compressive testing apparatuses, such as the Split Hopkinson Tension or Pressure Bars [6][7]. Most of these tests are carried out at room temperature, in some cases at higher temperatures to account for the cutting temperature increase, but none at sub-zero temperatures that the workpiece surface encounters during cryogenic machining.

To this regard, the objective of the paper is to show how the material behaviour changes when testing at sub-zero temperatures and elevated strain rate compared to conventional testing parameters. In the first part of the paper, a newly developed testing se-up, based on a Split Hopkinson Tension Bar, is presented, whereas the second part shows the

2212-8271
Peer-review under responsibility of the scientific committee of The 17th CIRP Conference on Modelling of Machining Operations
10.1016/j.procir.2019.04.160

experimental results in terms of flow stress and strain at fracture sensitivity to temperature and strain rate, as well as surface fracture features to evaluate the fracture modes at varying temperature.

2. Material and experimental procedures

2.1. Material under investigation

The material used in this study was the Ti6Al4V titanium alloy supplied in form of 1 mm thick sheets. The sheets were provided in annealed condition, characterized by an equiaxed α + β microstructure. According to the supplier's specification, the chemical composition of the Ti6Al4V alloy is reported in Table 1.

Table 1. Chemical composition of the Ti6Al4V titanium alloy (%wt).

Ti	Al	V	Fe	O	C	N
Balance	6	4	< 0.3	0.2	<0.08	<0.07

2.2. Split Hopkinson Tension Bar tests

To characterize the material behaviour at high strain rate, dynamic impact tests were carried out using a Split Hopkinson Tension Bar (SHTB) apparatus located at the L.A.M.I.H. laboratory in Valenciennes (France).

During the test, the sheet specimen is sandwiched between the incident pressure bar and the transmitter bar; a tensile load is produced by the release of a pre-stretched load at the end of the incident bar.

More details about the experimental procedure and analytical technique used to evaluate the dynamic mechanical response of the impacted specimens are presented in [8].

To match geometrical/material properties of the bars and the strain rates attended in this study, the shape of the specimens was accurately designed by means of analytical approaches [8].

Fig. 1 shows the drawing of the specimen used in this study. The specimens were laser cut from the as-received sheet along the rolling direction.

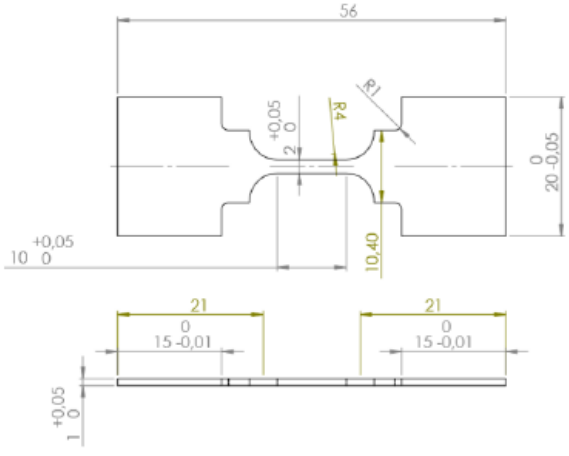

Figure 1. Drawing of the Ti6AlV sheet specimen used in this study (dimensions in mm).

Tests were performed at different strain rates and temperatures. In particular, strain rate values of 200 s^{-1} and 1000 s^{-1} were chosen as representative of machining processes, while the temperature was varied from 25°C to -150°C at steps of 50°C. In order to achieve sub-zero temperatures, a refrigeration chamber was specifically designed. The chamber is composed of an upper part and a lower part, in witch both the cylindrical bars and the sample are located in between. K-thermocouples are spot-welded on the sample' surface to measure the temperature during tests.

The experimental procedure adopted for sub-zero testing consists of the following three stages:

1. The lower part is placed below the connectors/bars set and the liquid nitrogen is completely spilled in. Then, the upper part is positioned over the lower part and a locking system assures the contact of the two parts. Five minutes of contact with the liquid nitrogen assures the specimen temperature close to -195°C.
2. The upper part is removed with the temperature still controlled by heat exchange with the environment. A mechanism is used to discharge the liquid nitrogen so that the connectors/sample set is no more immersed into the liquid nitrogen.
3. When the desired testing temperature is reached, the test is launched and data are collected.

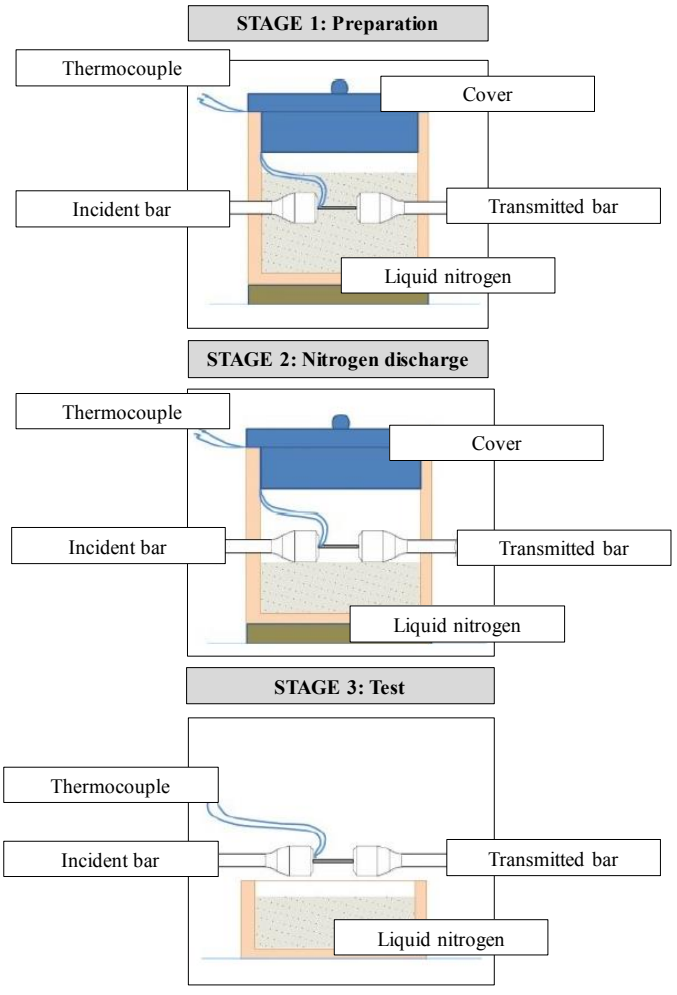

Figure 2. Experimental stages of SHTB tests under low temperatures regime.

The aforementioned three stages are schematically described in Fig. 2, while images of the experimental apparatus are reported on Fig. 3. From the latter, it can be seen that the chamber is large enough to ensure a constant temperature in the environment of the specimen.

It is supposed that a homogeneous temperature is obtained at the gauge area of the specimen thanks to its reduced dimensions. However, this information cannot be checked since the thermocouple is bonded at the surface of the specimen. It is also worth adding that the actual temperature during the test cannot be measured due to the very short time at break (less than 1ms).

Normally, a set of 3 tests was performed for each testing condition to ensure an acceptable repeatability of results and highlight possible material data dispersion at the same time.

For sake of comparison, quasi-static tests were carried out on a ElectroPuls™ Instron E 3000 machine with a strain rate of 0.008 s^{-1} at room temperature.

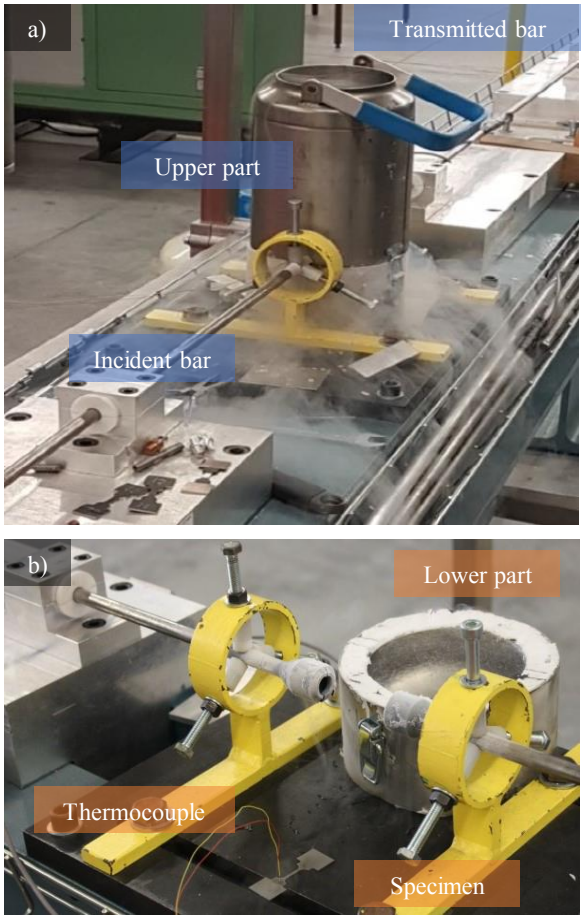

Figure 3. SHTB experimental setup apparatus: a) setting of the testing temperature in the refrigetation chamber; b) configuration after testing.

2.3. Characterization after SHTB tests

After SHTB tests, the specimens fracture surface was analyzed by means of a FEI™ QUANTA 450 Scanning Electron Microscope (SEM) using the Secondary Electron (SE) probe. Images at different magnifications, namely 5000X, 2000X and 1000X, were acquired.

Low magnification images of the fracture surfaces were acquired by SEM and the area was accurately measured by means of the length tool of the microscope.

3. Results and discussion

3.1. True stress–strain curves and strain at fracture

In this section, the Ti6Al4V mechanical behavior is presented with respect to different strain rates and temperatures. The flow stress relations are obtained using David™ software [9] on the basis on the governing equations mentioned in a previous paper [10]. For all the conditions, it is assumed a Poisson's coefficient of 0.34 and no visco-elasticity effect is considered.

Fig. 4 reports the effect of strain rate on the flow stress at room temperature. The tensile tests performed under dynamic conditions showed higher values of the fracture strength compared to the flow stress under quasi–static conditions, confirming the strain rate hardening effect at elevated strain rates. It is worth noting that the changes of the tensile tests strain rate do not influence significantly the elastic modulus of the investigated material: Young's modulus is 80 GPa in quasi-static conditions and close to 90 GPa under dynamic loadings. However, in the latter case, the elastic modulus cannot be accurately confirmed [11].

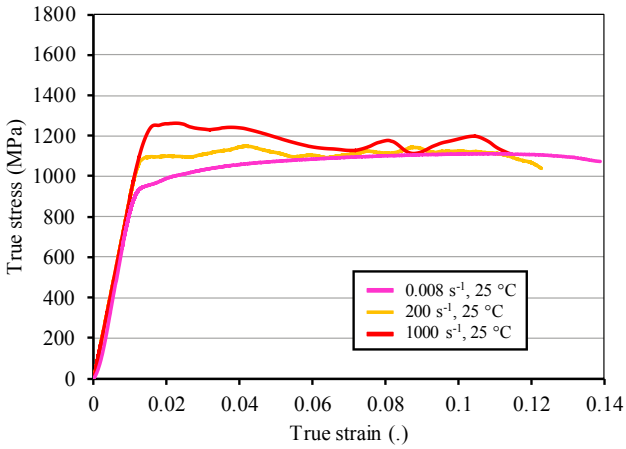

Figure 4. Ti6Al4V true stress–true strain curves as a function of strain rate at room temperature.

Fig. 5 a and b presents the Ti6Al4V true stress– true strain curves at strain rate of 200 s^{-1} and 1000 s^{-1}, respectively, and at temperatures varying from 25°C to -150°C. It can be clearly seen that the flow stress depends on both the strain rate and temperature. Specifically, at constant temperature, the flow stress increases rapidly at increasing strain rate, while at constant strain rate, the flow stress increases gradually at decreasing temperature [12].

For example, for a fixed true strain of 0.03 and strain rate of 200 s^{-1}, the flow stress increases from 1100 MPa to 1320 MPa as the temperature is reduced from 25°C to -150°C. Similarly, at the highest strain rate, the flow stress increases from 1210 MPa to 1580 MPa as the temperature is reduced from 25°C to -150°C. The curves shown in Fig. 6 show that

the strain rate governs not only the flow stress, but also the fracture strain.

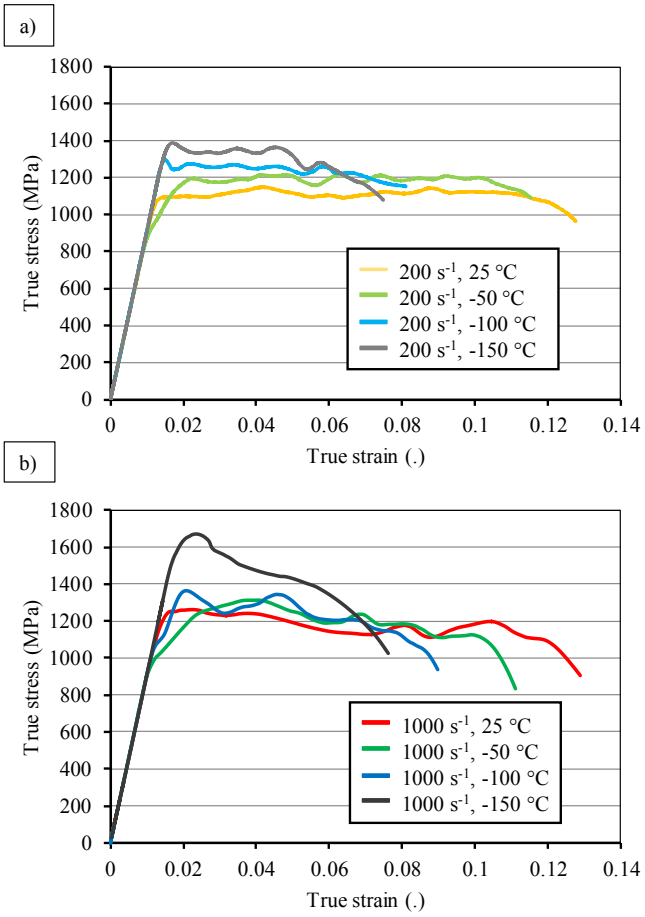

Figure 5. Ti6Al4V true stress–true strain curves as a function of temperature at a) 200 s^{-1} and b) 1000 s^{-1}.

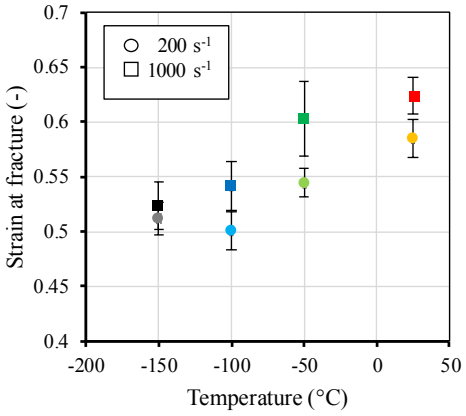

Figure 6. Ti6Al4V strain at fracture as a function of temperature at a) 200 s^{-1} and b) 1000 s^{-1}.

Specifically, at a given temperature, the fracture strain increases at increasing strain rate, but the effect is less evident at lower testing temperatures. On the other hand, at a constant strain rate, the fracture strain reduces drastically at decreasing reducing temperature, even if no sensible difference can be found between -100°C and -150°C.

3.2. Fracture surfaces

Figs. 7 and 8 report the SEM images of the specimens' fracture surfaces as a function of the strain rate and temperature at two different magnifications. Surface fractures are arranged in dimple-like features regardless of the testing parameters, thus indicating always a ductile fracture mechanism. It should be expected, that fracture nucleates in the area of α phase nucleation, then plastic flow occurs in the areas of β phase – much more ductile, close to α phase areas [13].

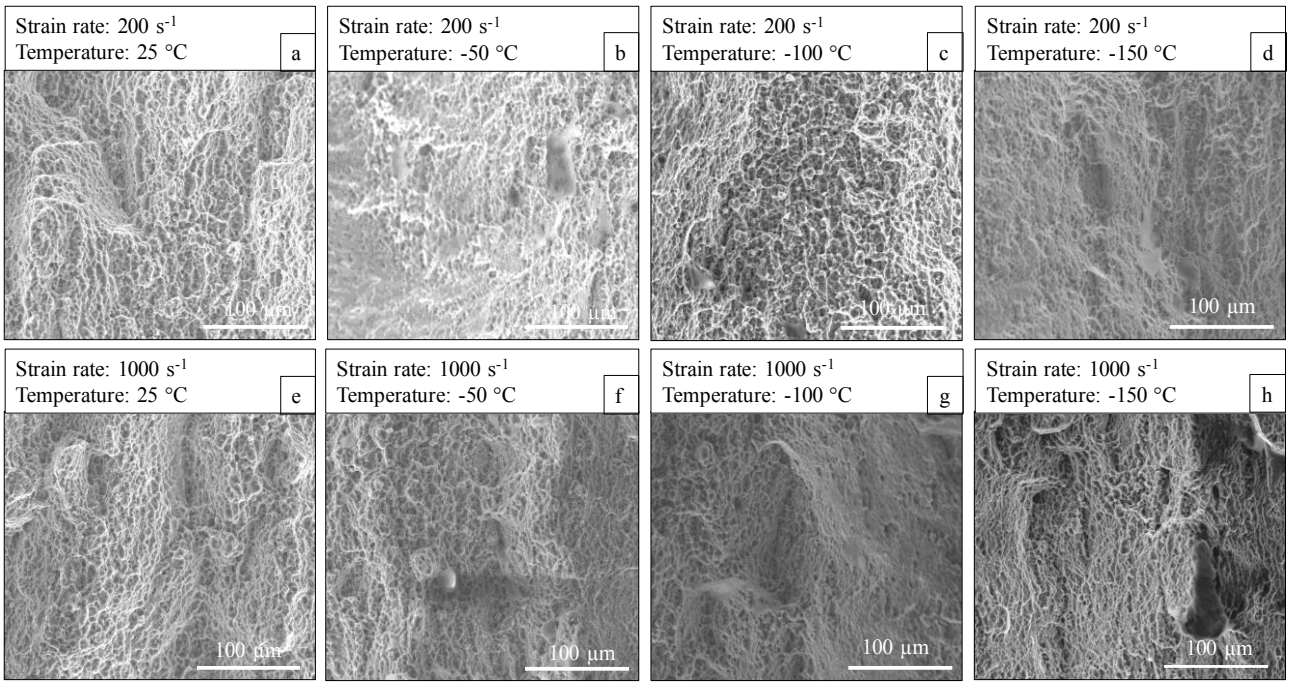

Figure 7. Fracture surfaces of the Ti6Al4V specimens deformed at different strain rates and temperatures (magnification 1000X).

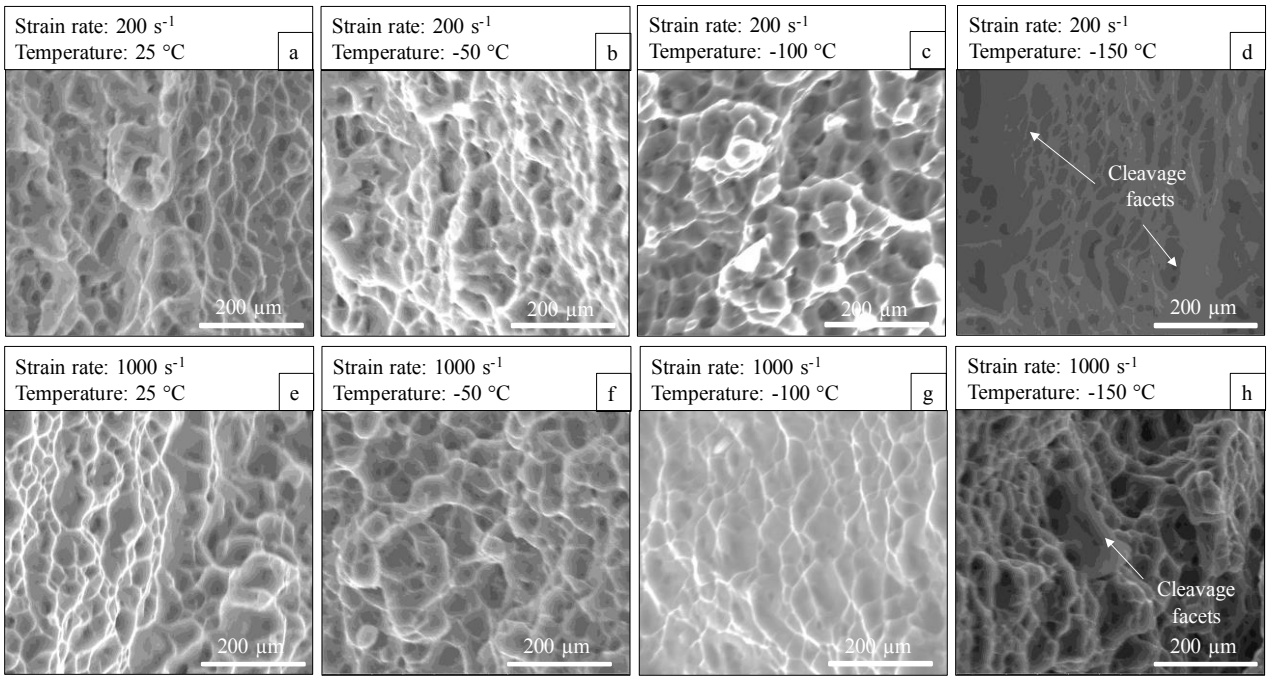

Figure 8. Fracture surfaces of the Ti6Al4V specimens deformed at different strain rates and temperatures (magnification 5000X).

Fig. 7 a and b presents the fractographies of the two specimens deformed at a temperature of 25 °C and strain rates of 200 s^{-1} and 1000 s-1, respectively.

The comparison of the two fracture surfaces shows that the dimple density increases at increasing strain rate. Similar tendencies are noted for the other testing temperatures and shown in in Fig. 7b, c and d.

On the contrary, the dimple density reduces and the number of flat cleavage planes increases as the temperature reduces. These more brittle features at the fracture surface are indicative of the hardening effects occurred when deforming at low temperatures and are a sign of reduced ductility. These findings are in accordance with the strain at fracture values reported in Fig. 6.

4. Conclusions

In this study the effect of the strain rate, up to 1000 s^{-1}, and temperature, in the range between 25°C and -150°C, on the Ti6Al4V mechanical behaviour was investigated.

To this purpose, a newly designed refrigeration chamber was designed to cool down the specimen for sub-zero testing and applied to the Split Hopkinson Tension Bar experimental apparatus.

The main findings can be summarized as follows:

- The material behaviour is sensitive to both strain rate and temperature. The flow stress increases with increasing strain rate and decreasing temperature. The strain rate and temperature effect on the strain at fracture is opposite.
- The SEM observations of the fracture surfaces show dimple structure indicative of a ductile rupture mechanism regardless of the strain rate and temperature adopted in this study. However, the dimple density increases as the strain rate is increased, while is reduced when deforming at sub-zero temperatures. Actually, at the lowest testing temperature cleavage surfaces are shown.

In future research, tests at elevated temperature at high strain rate will be conducted to take into account the temperature gradient that characterized the workpiece under machining operations.

References

[1] Jawahir IS, Attia H, Biermann D, Duflou J, Klocke F, Meyer D, Newman ST, Pusavec F, Putz M, Rech J, Schulze V, Umbrello D. Cryogenic manufacturing processes. CIRP Annals-Manuf Tech 2016;65/2:713–36.
[2] Sartori S, Bordin A, Bruschi S, Ghiotti A. Machinability of the EBM Ti6Al4V in Cryogenic Turning. Key Eng Mat 2015;651:1183-88.
[3] Bruschi S, Bertolini R, Ghiotti A, Savio E, Guo W, Shivpuri R. Machining-induced surface transformations of magnesium alloys to enhance corrosion resistance in human-like environment. CIRP Annals - Manuf Tech 2018; 67:579–582.
[4] Umbrello D, Bordin A, Imbrogno S, Bruschi S. 3D finite element modelling of surface modification in dry and cryogenic machining of EBM Ti6Al4V alloy. CIRP J Manuf Sci Tech 2017; 18:92–100.
[5] Rotella G, Umbrello D. Finite element modeling of microstructural changes in dry and cryogenic cutting of Ti6Al4V alloy, CIRP Annals – Manuf Tech 2014; 63/1:69–72.
[6] Denguir LA, Outeiro JC, Fromentin G, Vignal V, Besnard R. A physical-based constitutive model for surface integrity prediction in machining of OFHC copper. J Mat Process Tech 2017;248:143–160.
[7] Cheng W, Outeiro J, Costes JP, Saoubi R, Karaouni H, Denguir L, Astakhov V, Auzenat F. Constitutive model incorporating the strain-rate and state of stress effects for machining simulation of titanium alloy. Procedia CIRP 2018;77:344-7.
[8] Haugou G, Leconte N, Morvan H. Design of a pre-stretched tension Hopkinson bar device: Configuration, tail corrections, and numerical validation. Int J Impact Eng 2016;97:89–101.
[9] Gary G, Degreef V. DAVID, Users' manual version, Labview version. LMS Polytechnique, Palaiseau, France, version 12341.
[10] Achenbach J, Wave propagation in elastic solids. North-Holland, 1973.
[11] Safa K, Gary G. Displacement correction for punching at a dynamically loaded bar end. Int J Impact Eng 2010;37/4:371-384.

[12] Lee WS, Chen TH, Huang SC. Impact deformation behaviour of Ti–6Al–4V alloy in the low-temperature regime. J Nucl Mat 2010; 402:1-7.

[13] Wojtaszek M, Sleboda, T, Czulak A, Weber G, Hufenbach WA. Quasi-Static and Dynamic Tensile Properties of Ti-6Al-4V Alloy. Arch. Met. and Mat. 2013; 58:1261-5.